Comparison and Optimization of AVHRR Sea Surface Temperature Algorithms

I. J. BARTON AND R. P. CECHET

CSIRO Division of Atmospheric Research, Aspendale, Victoria, Australia

21 October 1988 and 1 May 1989

ABSTRACT

Satellite measurements of sea surface temperature (SST) are regularly available from data supplied by the AVHRR instruments on the NOAA meteorological satellites. In cloudless areas SST is derived from the infrared data using a differential absorption technique to correct for the effect of the atmosphere. For the AVHRR data a multichannel (multiwavelength) approach is used and global operational algorithms are in use. During 1990 a new instrument that has been specifically designed to measure SST will be launched on the European satellite, ERS-1. The Along Track Scanning Radiometer (ATSR) will provide six infrared measurements for each pixel on the earth's surface. Using the same differential absorption techniques, a multitude of algorithms for providing SST will then be possible. In this note a technique is described that will enable the comparison and optimization of SST algorithms and will also aid in the selection of the most appropriate algorithm for ATSR data analysis.

To demonstrate the technique mosaic images were constructed from small areas of cloud-free infrared images of the sea surface as seen by the NOAA-9 AVHRR. Each area was approximately 55 km by 55 km and, by arranging them in order of decreasing mean temperature and increasing mean zenith angle, it was possible to use an image analysis system to compare the relative performance of different algorithms for deriving surface temperature. The images were also used to compare some NOAA-7 SST algorithms.

A second set of mosaic images was constructed using NOAA-10 AVHRR data collected on the same night and for the same surface location. Images of SST derived with theoretical NOAA-10 algorithms were compared with those from an operational NOAA-9 algorithm. Then a simple optimization technique was used to obtain a new algorithm for deriving SST from channels 3 and 4 of the NOAA-10 instrument. This optimization scheme, using an ordered mosaic image that covers a wide range of conditions (location, local zenith angle, or some other parameter), should be applicable to the comparison and optimization of other satellite data products.

1. Introduction

Satellite measurements of sea surface temperature (SST) are now being used operationally in weather forecasting, oceanography, fishing, pollution monitoring and climate studies. Techniques for providing accurate measurements in clear sky conditions have now advanced to the stage where satellite estimates are as reliable as those supplied routinely by ships. Errors of 0.7 K in midlatitudes are possible with a larger error (1.0–2.0 K) in tropical regions. In 1990 the ERS-1 satellite to be launched by the European Space Agency will include the Along-Track Scanning Radiometer (ATSR) that has been designed to reduce the errors in the remote measurement of SST to about 0.3 K. This increased accuracy is due in part to the use of multiangle, as well as multichannel, measurements to determine the atmospheric absorption. With these forecast accuracies in SST, it will be necessary to take great care, not only in the derivation and validation of the algorithms, but also in the selection of the best algorithm to be used in each situation.

The current operational multichannel (MCSST) algorithms are obtained initially from a theoretical atmospheric transmission model and then fine tuned using coincident satellite and drifting buoy data. For the NOAA series of satellites SST has been derived using the split window channels (4 and 5) of the Advanced Very High Resolution Radiometer (AVHRR) instrument. These channels have a bandwidth of 1 μm and are centered at wavelengths of 10.8 and 12.0 μm, respectively. Although a more accurate SST measurement should be available by using AVHRR channel 3 at 3.7 μm with channel 4, algorithms using these channels have not been used as the 3.7 μm channels of past AVHRR instruments have developed a noisy signal soon after launch.

In this note we give an example of a technique that can be used for both comparison and optimization of new algorithms for deriving SST from satellite data. This is done by using a mosaic of small clear sky images of the sea surface that covers a range of view angles from nadir to the edge of the AVHRR swath and from tropical seas to those with temperatures near 13°C. The relative performances of different algorithms for

Corresponding author address: Dr. I. J. Barton, CSIRO/Division of Atmospheric Research, Private Bag No. 1, Mordialloc, Victoria 3195, Australia.

NOAA-7 and NOAA-9 are discussed and an SST algorithm for NOAA-10 AVHRR is derived. This latter algorithm is compared with one obtained using an atmospheric transmission model.

Early in the life of the ATSR mission it will be necessary to compare the derived SST fields with those obtained from the operational AVHRR instruments. The technique described here will provide a useful means of comparing the relative performance of the two different instruments. The ATSR has effectively six infrared channels (3.7, 10.8 and 12 μm at two different view angles) and thus a multitude of SST algorithms is possible using 2–6 measurements for each pixel. This technique will then assist in the selection of the best ATSR SST algorithm depending on such factors as location, atmospheric water vapor content, surface wind speed and atmospheric aerosol content.

The algorithms used in the NOAA-9 analysis are also compared using collocated satellite and ship data collected in Australian waters. This comparison highlights the problems encountered in deriving SST in tropical areas. The technique described here could be used to derive a better algorithm for use in tropical waters.

2. Satellite datasets

Large areas of NOAA-9 AVHRR data from a range of latitudes and containing cloudless areas over the sea were collected. A simple signal threshold and spatial coherence technique was then used to select smaller areas over the sea that were apparently cloud-free. Each of these small areas was then mapped onto a latitude–longitude grid of approximately 55 km by 55 km (50 $\times$ 50 grid points). The satellite measured radiances were converted to brightness temperatures using a Planck function with an appropriate wavelength. One hundred small areas were then used to generate mosaic images of the brightness temperatures in the three NOAA-9 infrared channels. The data were all from nighttime passes so that the 3.7 micrometer channel (No. 3) was not contaminated with reflected solar radiation. The current AVHRR instruments have an inherent periodic noise in the channel 3 data that appears to increase with the age of the satellite. In our data this noise was reduced by passing the raw data stream through a filter, but when viewing the mosaic images it was obvious that some of the noise remained (for example, see Fig. 2). The mosaic elements were arranged so that the brightness temperatures were highest at the top and lowest at the bottom of the mosaic and the observation angle (zenith angle) increased from left to right. This arrangement could then be used to investigate the relative performance of different NOAA-9 SST algorithms for different temperatures and view angles. Figure 1 shows the mosaic image of the satellite brightness temperature in channel 4, the average SST of each element as calculated with the NOAA-9 MCSST algorithm (E. P. McClain 1986, private communication) and the zenith angle at the earth's surface.

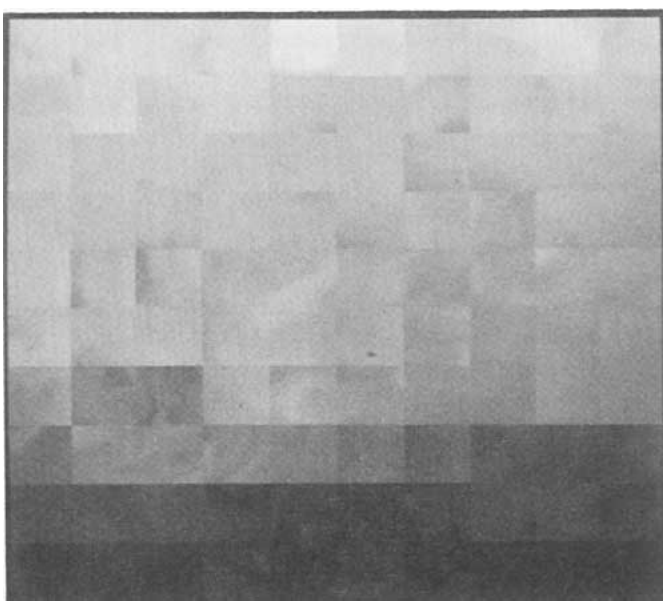

20.7 (2)	20.8 (9)	20.7 (29)	20.9 (32)	22.5 (49)	21.6 (52)	20.8 (52)	20.9 (54)	21.9 (54)	20.8 (57)
19.9 (1)	20.6 (1)	20.1 (9)	20.5 (11)	19.9 (13)	19.9 (14)	20.0 (26)	20.6 (29)	20.6 (30)	20.6 (39)
19.9 (2)	19.6 (5)	19.7 (9)	19.6 (17)	19.6 (20)	19.8 (21)	19.6 (35)	19.5 (47)	19.7 (50)	19.8 (57)
19.2 (6)	19.1 (8)	19.0 (13)	19.3 (22)	19.2 (22)	19.3 (23)	19.5 (23)	19.2 (24)	19.5 (52)	19.3 (56)
19.0 (16)	18.7 (16)	18.7 (17)	18.8 (18)	18.8 (21)	19.1 (22)	18.8 (23)	18.9 (24)	19.2 (25)	19.2 (53)
18.7 (9)	18.5 (11)	18.6 (11)	18.6 (15)	18.5 (21)	18.5 (21)	18.5 (34)	18.6 (56)	18.6 (57)	18.7 (58)
16.9 (2)	16.5 (14)	16.2 (17)	17.8 (24)	18.3 (26)	17.7 (27)	17.6 (56)	17.8 (57)	18.3 (57)	18.3 (58)
15.1 (9)	16.1 (24)	16.2 (24)	16.4 (26)	15.8 (27)	15.6 (29)	14.9 (30)	14.8 (30)	14.5 (30)	15.3 (31)
13.6 (10)	13.5 (11)	13.5 (14)	12.8 (21)	12.8 (22)	12.7 (24)	13.5 (27)	14.3 (31)	14.3 (32)	14.3 (33)
12.6 (18)	12.6 (22)	12.0 (22)	12.2 (24)	11.9 (25)	12.5 (25)	12.1 (27)	12.3 (34)	12.5 (36)	12.6 (36)

FIG. 1. (a) The mosaic image for the NOAA-9 AVHRR channel 4 brightness temperature. Dark areas are cold (12°C) and light areas hot (22°C). (b) The corresponding average SST (in °C) for each mosaic element as derived with the MCSST algorithm for the NOAA-9 data, and the satellite zenith angle in degrees as viewed from the surface (in brackets).

A closer look at the mosaic images reveals that some of the elements display large gradients in brightness temperature. Because the same gradients appear in the NOAA-10 data (collected either 8 hours earlier or 3 hours later) we are confident that the cloud detection technique works well and that the gradients are in SST and are not due to clouds. There are, however, three or four small areas toward the bottom of the mosaic that are most likely due to islands or isolated clouds but have passed through our cloud detection test. These small areas are less than 5 × 5 pixels in size, have a brightness temperature not too different to the surrounding area, and will thus have no significant effect on the following analysis.

A second set of mosaic images was created by taking the data from the NOAA-10 satellite orbit that covered the same area as either the preceding or following NOAA-9 orbit. The small areas corresponding to those used in the NOAA-9 mosaic were checked to ensure that they were also cloud-free and were then remapped onto the same latitude–longitude grid as the NOAA-9 data. The NOAA-10 mosaic images were generated by placing the elements in the same mosaic location as the corresponding NOAA-9 elements. In the NOAA-10 mosaic images the temperature gradation from the top to the bottom of the image was maintained, but the view angle ordering was destroyed as the NOAA-10 angles bear no simple relation to the corresponding NOAA-9 data. NOAA-10 data were collected either after sunset or just after sunrise. In the latter case the sun angle was sufficiently low so that reflected solar radiation did not contribute significantly to the radiance at 3.7 μm. NOAA-10 carries the 4-channel version of the AVHRR and so only two infrared images were created; channel 3 centered at 3.7 μm and channel 4 at 10.8 μm.

The spectral response functions for the same channel on different AVHRR instruments are slightly different, resulting in the need for different SST algorithms for each satellite.

3. Algorithm comparison

a. NOAA-9

The NOAA-9 MCSST algorithm was taken as the standard in this comparison; i.e., the correct SST is derived using the following algorithm with T_4 and T_5 being the brightness temperatures in absolute degrees:

$$\text{SST} = 3.703T_4 - 2.704T_5 + 0.71 \quad \text{(M45)} \quad (1)$$

[The code M45 refers to the McClain channels 4 and 5 algorithm; B refers to Barton et al. (1989), and θ, used in the codes below, refers to an algorithm that has a view angle dependence.]

For NOAA-9 the MCSST algorithm was tested against those derived by Barton et al. (1989) from a band model of atmospheric absorption. The McClain algorithms have been kindly supplied by E. P. McClain of NOAA/NESDIS. Comparisons with the accepted "true SST" were made with the SST derived using algorithms with a view-angle dependence and those independent of view angle. Comparisons were also made with SSTs derived with algorithms using channels 3 and 4. The algorithms used were:

$$\text{SST} = 3.638T_4 - 2.634T_5 - 0.46 \quad \text{(B45)} \quad (2)$$

$$\text{SST} = \text{SST(M45)} - 0.27S(T_4 - T_5) + 0.738S - 0.23 \quad \text{(M45}\theta\text{)} \quad (3)$$

$$\text{SST} = (3.439 + 0.853S)T_4 - (2.429 + 0.845S)T_5 - (2.07 + 1.70S) \quad \text{(B45}\theta\text{)} \quad (4)$$

$$\text{SST} = 1.525T_3 - 0.512T_4 - 1.54 \quad \text{(M34)} \quad (5)$$

$$\text{SST} = 1.494T_3 - 0.454T_4 - 9.15 \quad \text{(B34)} \quad (6)$$

$$\text{SST} = \text{SST(M34)} + 0.958S(T_3 - T_4) + 1.550S - 0.32 \quad \text{(M34}\theta\text{)} \quad (7)$$

$$\text{SST} = (1.439 + 0.083S)T_3 - (0.395 + 0.071S)T_4 - (10.51 + 1.80S) \quad \text{(B34}\theta\text{)} \quad (8)$$

where $S = \sec(\theta) - 1$, θ being the zenith angle of the satellite at the earth's surface.

For each of these algorithms the differences between the SSTs for M45 and the algorithm concerned were analyzed in image form. The standard deviations and average biases for the SST difference images are given in Table 1, which also contains some results for differences not included in the following discussion. It was also possible to view the difference images (e.g., Fig. 2 for M45 − M34) to compare the relative performance at a range of surface temperatures and zenith angles.

Because the coefficients are quite similar there is no significant difference between the M45 and B45 algorithms. The difference image shows a uniform value of near 0.2 K at all temperatures and zenith angles.

The difference image for the M45 and M45θ algorithms show that the agreement is good at all temperatures and zenith angles, but is best for high and low temperatures at low and high angles and is worst (approximately 0.12 K only) at medium temperatures and middle angles.

The M45 − B45θ SST difference image shows low values for all image locations except for high temperatures at low and high angles where the difference value is near 0.9 K.

The M45 − M34 SST difference image is shown in Fig. 2. Assuming that the M45 algorithm provides the correct value of SST, the M34 algorithm performs best for both high and low SST values with larger zenith angles and performs reasonably well for other temperatures and zenith angles except for high temperatures and low zenith angles. The M45 − B34 comparison showed a similar difference image to that for M45 − M34.

TABLE 1. Difference image statistics for the algorithm intercomparison. See the text for codes.

Difference image details	Mean bias (K)	Standard deviation (K)
NOAA-9		
M45 − B45	−0.22	0.01
M45 − M45θ	0.16	0.07
M45 − B45θ	−0.36	0.20
B45 − B45θ	−0.14	0.20
M45 − M34	0.68	0.63
M45 − B34	0.55	0.60
M45 − B34θ	0.52	0.56
M34 − B34	−0.13	0.07
M34 − B34θ	−0.16	0.27
B34 − B34θ	−0.03	0.24
NOAA-10		
M45(NOAA-9) − B10	−0.28	0.77
M45(NOAA-9) − B10θ	−0.32	0.77
M34(NOAA-9) − B10	−0.96	1.03
M34(NOAA-9) − B10θ	−1.00	1.04
B10 − B10θ	−0.04	0.21
NOAA-7 (Channels 4 and 5)		
MCSST (night) − MCSST (day)	−0.31	0.22
− Imbault	0.79	0.56
− Singh (1984)	0.25	0.66
− Maul (1983)	−1.40	0.19
− Minnett et al. (1982)	−1.20	0.31
− Llewellyn-Jones et al. (1984)	0.96	0.29

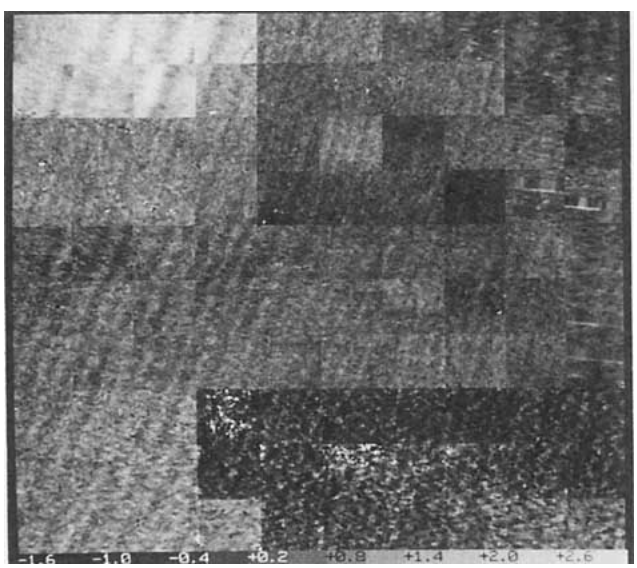

FIG. 2. The NOAA-9 difference image for the SSTs derived with the MCSST and the McClain channels 3 and 4 algorithm. The gray scale shows the difference between the SST calculated with the two algorithms (°C). The striations in the image result from the periodic noise in channel 3, which has not been completely removed by the filtering process.

M34 was also compared to B34 and B34θ. As expected the agreement was quite good for the first of these due to the similarity between the two algorithms. The second difference image showed good agreement except for high temperatures at low and high zenith angles.

In a later section the use of this analysis technique is used to derive an optimum set of coefficients for channels 3 and 4 algorithms for the NOAA-10 AVHRR instrument.

b. *NOAA-10*

The NOAA-10 algorithms used for comparison were derived in the same manner as those for the NOAA-9 using the band model of Barton et al. (1989) with the NOAA-10 AVHRR filter response functions. The algorithms derived were:

$$\text{SST} = 1.411T_3 - 0.375T_4 - 7.87 \quad \text{(B10)} \quad (9)$$

$$\text{SST} = (1.367 + 0.070S)T_3 - (0.327 + 0.059S)T_4 - (9.228 + 1.494S) \quad \text{(B10}\theta\text{)}. \quad (10)$$

The statistics for the NOAA-10 comparisons are also included in Table 1. In the first four of these comparisons we assume that the SST derived with the NOAA-

9 algorithms and the NOAA-9 data are the true SST values for the NOAA-10 images. This is a reasonable assumption as the SST does not change significantly in the 3 or 8 hour period between the collection of the two sets of data, and each of the elements of the NOAA-10 mosaic matches the corresponding NOAA-9 element. In the NOAA-10 comparisons no deductions can be made with regard to the performance at different zenith angles as the images are no longer ordered in increasing angle from left to right.

The M45 − B10 difference image shows the best agreement for middle values of temperature, negative values up to 2 K at high temperatures and positive values for low temperatures. There was no significant improvement in the comparison for the M45 − B10θ difference.

c. NOAA-7

The performance of several NOAA-7 SST algorithms for channels 4 and 5 was assessed. In this comparison we assume that the NOAA-7 satellite brightness temperatures are the same as those for the NOAA-9 mosaics. The McClain nighttime MCSST algorithm was again assumed to produce the "true SST" against which all other algorithms were compared. The algorithms used are:

$$\text{SST} = 4.244T_4 - 3.168T_5 - 23.07 \quad \text{(MCSST, night)} \quad (11)$$

$$\text{SST} = 3.614T_4 - 2.580T_5 - 10.05 \quad \text{(MCSST, day)} \quad (12)$$

$$\text{SST} = 2.270T_4 - 1.270T_5 - 0.18 \quad \text{(Imbault et al. 1981)} \quad (13)$$

$$\text{SST} = 1.764T_4 - 0.764T_5 - 0.78 \quad \text{(Singh 1984)} \quad (14)$$

$$\text{SST} = 4.350T_4 - 3.350T_5 + 0.32 \quad \text{(Maul 1983)} \quad (15)$$

$$\text{SST} = 3.573T_4 - 2.575T_5 + 0.79 \quad \text{(Minnett et al. 1982)} \quad (16)$$

$$\text{SST} = 3.795T_4 - 2.803T_5 - 1.48 \quad \text{(Llewellyn-Jones et al. 1984).} \quad (17)$$

The statistics of the difference images are given in Table 1. The difference image between the night and day MCSST algorithms showed a value of −0.2 K for all areas except those for low temperatures and high angles where the values were near −0.6 K. In all other cases there was a general diagonal gradation in difference from larger values at high temperature/low angle (top left of the image) to smaller values at low temperature/high angle (bottom right). For example, the MCSST/Llewellyn-Jones difference was 1.4 K at the top left, decreasing to 0.4 K at the bottom right, while the MCSST/Maul difference was 1.4 K at the top left and −1.8 K at the bottom right.

4. Derivation of NOAA-10 SST algorithm

The comparison between the MCSST values (derived for NOAA-9) and the B10 algorithm (derived from theory for NOAA-10 channels 3 and 4), gives a bias of −0.28 K and a standard deviation of 0.77 K. An optimization procedure based on least-squares was used to find the best simple algorithm for deriving SST (i.e., matching the MCSST values). The coefficients of T_3 and T_4 in the B10 algorithm [Eq. (9)] were each adjusted until the standard deviation of the temperature difference image was a minimum (0.68 K). The optimized values of the coefficients are given in the following algorithm:

$$\text{SST} = 1.30T_3 - 0.38T_4 + 25.68. \quad (17)$$

TABLE 2. Satellite brightness temperatures and ship data for the algorithm intercomparison.

NOAA-9 orbit (*: daytime)	Date (d/mo/yr)	Location		Ship SST	Satellite brightness temperatures		
		Latitude (°S)	Longitude (°E)		T_3	T_4	T_5
4 467*	25/10/85	18.4	153.5	26.7	—	19.9	17.7
4 510*	28/10/85	15.6	156.5	28.4	—	15.6	12.5
4 524*	29/10/85	13.4	154.9	29.1	—	19.1	16.0
4 545	31/10/85	13.0	151.7	27.4	—	22.9	21.4
4 552*	31/10/85	13.5	150.7	27.4	—	22.5	20.7
4 559*	01/11/85	14.3	149.3	26.9	—	18.5	16.3
4 580*	02/11/85	14.4	146.0	26.6	—	16.2	13.7
4 602	04/11/85	16.6	147.7	26.5	—	17.9	15.1
13 942	27/08/87	29.1	113.8	20.5	17.3	17.9	17.4
13 956	29/08/87	28.2	113.8	19.7	17.5	16.6	15.3
13 970	30/08/87	29.1	114.0	20.3	17.3	16.4	15.1
14 069	06/09/87	29.1	114.5	18.9	17.2	17.1	16.1
14 083	07/09/87	30.1	114.6	19.2	16.9	17.3	16.7

For comparison, the optimized and original algorithms were also compared in the usual manner. The difference image (B10–optimum) shows a bias of 0.22 K and a standard deviation of 0.38 K.

This simple optimization procedure in fact gave a large range of values (with the sum of the two coefficients being close to unity) over which the standard deviation changed little. This insensitivity of bichannel SST algorithms to the actual value of the two brightness temperature coefficients is also evident in the NOAA-7 algorithms given above in Eqs. (11)–(17). The major constraint is for the sum of the coefficients to be near unity.

5. Comparisons using collocated ship and satellite data

Data collected during two cruises of the R.V. *Franklin* were used to further test the performance of the NOAA-9 algorithms. Details of the ship and satellite data are given in Table 2. During both cruises the ship SST measurements were obtained with a calibrated thermosalinograph that was regularly checked with bucket measurements and an accurate thermistor. The SST values calculated using the various NOAA-9 algorithms are given in Table 3. For each algorithm the bias and standard deviations are given for the total dataset as well as just for the midlatitude data.

The intercomparison of these different algorithms is complicated by the presence of a cool skin layer at the ocean surface (Paulson and Simpson 1981). Robinson et al. (1984) report that in the case of a well-mixed surface layer the bulk temperature of the ocean is warmer than the radiative temperature of the surface skin layer by 0.1–0.5 K. The McClain algorithms are fine-tuned using coincident satellite and buoy data and thus give a measure of the bulk temperature. The Bar-

TABLE 3. Comparison of ship data with SSTs calculated from the various NOAA-9 algorithms. Temperatures are in °C. The figures in brackets show the difference between the ship and algorithm SST.

Orbit	Zenith angle (°C)	Ship SST	M45	B45	M45θ	B45θ	M34	B34	M34θ	B34θ
4 467	50	26.7	26.3 (0.4)	26.4 (0.3)	26.1 (0.6)	27.5 (−0.8)				
4 510	65	28.4	24.4 (40.0)	24.5 (3.9)	24.0 (4.4)	28.4 (0.0)				
4 524	54	29.1	27.9 (1.2)	28.0 (1.1)	27.6 (1.5)	29.8 (−0.7)				
4 545	36	27.4	27.4 (0.0)	27.6 (−0.2)	27.2 (0.2)	27.9 (−0.5)				
4 552	5	27.4	27.8 (−0.4)	28.0 (−0.6)	27.6 (−0.2)	27.8 (−0.4)				
4 559	56	26.9	24.9 (2.0)	25.0 (1.9)	24.8 (2.1)	26.7 (0.2)				
4 580	60	26.6	23.4 (3.2)	23.5 (3.1)	23.2 (3.4)	25.8 (0.8)				
4 602	43	26.5	25.9 (0.6)	26.0 (0.5)	25.7 (0.8)	26.6 (−0.1)				
13 942	10	20.5	19.7 (0.8)	19.9 (0.6)	19.5 (1.0)	20.0 (0.5)	19.2 (1.3)	19.5 (1.0)	18.9 (1.6)	19.4 (1.1)
13 956	29	19.7	20.5 (−0.8)	20.7 (−1.0)	20.4 (−0.7)	20.8 (−1.1)	20.2 (−0.5)	20.4 (−0.7)	20.2 (−0.5)	20.4 (−0.7)
13 970	40	20.3	20.3 (0.0)	20.5 (−0.2)	20.2 (0.1)	20.9 (−0.6)	20.0 (0.3)	20.2 (0.1)	20.4 (−0.1)	20.5 (−0.2)
14 069	0	18.9	20.2 (−1.3)	20.4 (−1.5)	20.0 (−1.1)	20.4 (−1.5)	19.5 (−0.6)	19.7 (−0.8)	19.2 (−0.3)	19.5 (−0.6)
14 083	15	19.2	19.3 (−0.1)	19.6 (−0.4)	19.1 (0.1)	19.6 (−0.4)	18.9 (0.3)	19.2 (0.0)	18.6 (0.6)	19.1 (0.1)
All data										
		Bias	0.74	0.58	0.94	−0.35				
		Standard error	1.65	1.62	1.78	0.70				
Midlatitude data										
		Bias	−0.28	−0.74	−0.12	−0.62	0.16	0.08	0.26	0.06
		Standard error	0.77	0.87	0.74	0.92	0.70	0.65	0.81	0.65

ton et al. (1989) algorithms are derived using a model of infrared transmission through the atmosphere and therefore give the skin temperature. Thus, ideally, the McClain temperatures should agree exactly with the ship data while the Barton temperatures should underestimate by about 0.3 K.

The set of atmospheric profiles used by Barton et al. (1989), although containing a spread of data for all latitudes, are biased towards tropical maritime atmospheres. This is probably the reason for the good agreement between the theory and observations for the B45θ algorithm. The other algorithms, M45, B45 and M45θ, all perform poorly on the tropical data but do quite well on the midlatitude data. As expected, the differences between the biases of the algorithms is in close agreement with the image analysis above. These results suggest that it may be necessary to use a modified MCSST algorithm for tropical areas. The results here also indicate that similar accuracies may be obtainable for tropical areas as for midlatitudes. From this small dataset the error in satellite derived SST using AVHRR channels 4 and 5 appears to be near 0.8 K.

6. Concluding remarks

As numerical models of the ocean and atmosphere become more sophisticated, so the datasets used for initialization and verification will require better accuracy and broader coverage. Satellite instrumentation will be able to supply these datasets only if techniques exist that can accurately analyze the satellite data. A method of using an interactive image analysis system to assess the performance of different algorithms for deriving SST is described in this note. Here the data have all been collected off the east coast of Australia between latitudes of 15° and 40°S and so there may be a geographical bias to this algorithm analysis. For global algorithms a dataset that includes a larger range of sea surface temperatures and locations is required.

In the example given in this note we have used channel 4 brightness temperature and local zenith angle as the two parameters to create the order of our mosaic image. Future analyses could well use other parameters of interest: e.g., aerosol content, surface wind speed and atmospheric water vapor content.

This analysis will be further developed for the intercomparison of SST fields derived from operational AVHRR instruments on the NOAA satellites and the products from the ATSR. For the ATSR data analysis it is most likely that different algorithms will be used to derive SST depending on several factors including location, time of day, local weather conditions and atmospheric aerosol content. By using this mosaic technique it will be possible to assess the performance of different algorithms under different conditions.

The technique should also find parallel uses in the intercomparison and optimization of many other satellite-derived products.

REFERENCES

Barton, I. J., A. M. Zavody, D. M. O'Brien, D. R. Cutten, R. W. Saunders and D. T. Llewellyn-Jones, 1989: Theoretical algorithms for satellite-derived sea surface temperatures. *J. Geophys. Res.*, **94,** 3365–3375.

Imbault, D., N. A. Scott and A. Chedin, 1981: Multi-channel radiometric determination of sea surface temperature: Parameterization of the atmospheric correction. *J. Appl. Meteor.*, **20,** 556–564.

Llewellyn-Jones, D. T., P. J. Minnett, R. W. Saunders and A. M. Zavody, 1984: Satellite multi-channel infrared measurements of sea surface temperature of the N.E. Atlantic Ocean using AVHRR/2. *Quart. J. Roy. Meteor. Soc.*, **110,** 613–631.

Maul, G. A., 1983: Zenith angle effects in multi-channel infrared sea surface remote sensing. *Remote Sens. Environ.*, **13,** 438–451.

Minnett, P. J., R. W. Saunders, A. M. Zavody and D. T. Llewellyn-Jones, 1982: Performance of the split-window at 11 and 12 μm wavelengths for accurate determination of sea surface temperature. *Ann. Meteor.*, **18,** 58–60.

Paulson, C. A., and J. J. Simpson, 1981: The temperature across the cool skin of the ocean. *J. Geophys. Res.*, **86,** 11 044–11 054.

Robinson, I. S., N. C. Wells and H. Charnock, 1984: The sea surface thermal boundary layer and its relevance to the measurement of sea surface temperature by airborne and spaceborne radiometers. *Int. J. Remote Sens.*, **5,** 19–45.

Singh, S. M., 1984: Removal of atmospheric effects on a pixel by pixel basis from the thermal infrared data from instruments on satellites. The Advanced Very High Resolution Radiometer (AVHRR). *Int. J. Remote Sens.*, **5,** 161–183.